Out-plane Buckling of Arches with Variable Cross-section

Angfeng Jiang , Deyuan Deng , Wei Dai , Xiuwen You , Hanwen Lu *

Posted Date: 13 October 2023

doi: 10.20944/preprints202310.0874.v1

Keywords: variable cross-section; arch; critical out-plane buckling load; uniformly distributed radial local load

Article

Out-Plane Buckling of Arches with Variable Cross-section

Angfeng Jiang [1], Deyuan Deng [2,3], Wei Dai [3], Xiuwen You [3] and Hanwen Lu [1,*]

[1] School of Transportation and Civil Engineering & Architecture, Foshan University, Foshan 528225, China
[2] School of Civil Engineering, Southeast University,Nanjing 211189,China
[3] China Construction Steel Structure Guangdongcorp.ltd., Huizhou 516200, China
* Correspondence: hanwenlo@foxmail.com

Abstract: Variable cross-section arch is widely used in practical engineering because of its beautiful arc and excellent mechanical properties. However, there is still no systematic and comprehensive study on the out-plane buckling of variable cross-section arch. In view of this, this paper is concentrated on an elastic analytical research of out-plane buckling of arches with variable cross-section under a uniformly distributed radial local load. The pre-buckling and out-plane buckling behaviour of a variable cross-sectional arch under an external load is quite different from that of an arch with uniform cross-section. The Castigliano's second theorem is used to establish pre-buckling force method equilibrium equations for variable cross-sectional arches under a uniformly distributed radial local load, and corresponding analytical solutions of normal stress, axial compression and the bending moment are obtained. Based on the energy method and the Ritz method, analytical solutions of the critical load for the elastic out-plane buckling of arches with variable cross-section are derived. Comparisons with ANSYS results indicated that the analytical solutions are able to accurately predict the pre-buckling internal forces and critical out-plane buckling load of variable cross-section arches subjected to a uniformly distributed radial local load. It is found that the internal forces and the out-plane buckling load of an arch are significantly affected by the variation of cross-sectional height. With the ratio of cross-sectional height of the top to the end increase, the bending moment decreases and the axial force and critical out-plane buckling load increase. Analytical solutions of pre-buckling internal force and critical out-plane buckling load problems for arches with variable cross-section have a wider significance, since they can provide an effective explicit analytic method for the optimal design of arch structure.

Keywords: variable cross-section; arch; critical out-plane buckling load; uniformly distributed radial local load

1. Introduction

In the design of arch structures, the form of variable cross-section is widely used, and the elastic internal force and critical out-plane buckling load are essential to derive modified slenderness for out-plane stability design. Most of the previous studies focused on uniform cross-section arches for their out-plane buckling. For various load patterns, the out-plane buckling behavior of arch structure has been investigated by several researchers.. Trahair[1], Liu et al[2], and Yuan et al[3] examined the out-plane buckling of arches which subjected to uniformly distributed loads. Pi et al[4] focused on investigating the out-plane buckling of arches under a central concentrated load. Liu and Lu et al[5,6] conducted studies on the out-plane lateral and torsional instability of arches under arbitrary radial concentrated loads and a central radial point load. In order to better simulate the load patterns observed in actual engineering scenarios, Lu et al[7] investigated the flexural-torsional buckling of steel arches subjected to a localized uniform radial load. For various constraint boundaries, Pi and Bradford[8] introduced a design equation that predicts the out-plane strengths of fixed steel arches. Guo et al[9] developed analytical solutions for the out-plane buckling load of arches with elastic end

 doi:10.20944/preprints202310.0874.v1

restraints. Additionally, Xi et al[10] conducted a buckling analysis of pin-end arches. For various materials, Pi and Trahair[11] conducted theoretical derivations and finite element research on the out-plane inelastic buckling and strength of steel arches. Bouras and Vrcelj[12] investigated the out-plane buckling behavior of concrete-filled steel tubular arches which are studied in elevated temperatures. Liu et al[13] explored the out-plane buckling of functionally graded porous I-shaped circular arches with graphene platelet reinforcements. For various cross-sections, Malekzadeh and Karami[14] conducted an out-plane static analysis of an arch with circular cross-section. Lim and Kang[15] investigated the out-plane buckling of I-shaped arches with a single symmetric axis cross-section, while Xi et al[16] studied the out-plane buckling of I-shaped arches with a double symmetric axis cross-section. Wang et al[17] examined the out-plane buckling and in-plane buckling of an arch with a box cross-section. Guo et al[18] developed methods for determining the out-plane inelastic strength of trussed arches with a rectangular lattice cross-section. Furthermore, Zhong et al[19] provided theoretical solutions and experimental studies on a rectangular cross-section arch. In addition to the aforementioned studies, there have been numerous investigations on the out-plane buckling of arches considering various factors such as shearing effects[20], temperature fields[21], creep[22,23], and functionally graded materials[24,25]. However, due to the scope of this paper, not all of these studies will be introduced.

From the existing literature, it is evident that arches with uniform cross-sections have been extensively studied, while only a limited number of studies have focused on arches with variable cross-sections. Huang et al.[26] investigated the in-plane vibration of circular arches which has variable curvature and variable cross-sections. Shin et al.[27] optimized the vibration analysis of circular arches with variable cross-sections. Tsiatas and Babouskos[28] studied the linear and nonlinear responses of non-uniform shallow arches subjected to concentrated forces and developed corresponding integral equation solutions. More recently, Yan et al.[29,30] conducted an in-depth study on the buckling behavior of non-uniform arches divided into three regions with constant stiffness. However, there is a lack of research in the literature concerning the out-plane buckling of arches with variable cross-sections under locally uniform radial loads.

In order to further investigate the elastic analysis of out-plane buckling of a variable cross-section arch under a uniformly distributed radial local load, this paper resorts to the Timoshenko beam theory and Castigliano's second theorem, and proposes an exponential variable cross-sectional form based on the natural constant e to solve normal stress, axial compression and bending moment of the variable cross-sectional arch before buckling. Based on the precise axial compression and bending moment, the analytical solution of critical out-plane buckling load of variable cross-sectional arch is derived, and the numerical model was obtained with ANSYS software to verify the accuracy of the analytical solution. It provides an effective explicit analysis method for the optimal design of arch structure.

2. Basic assumptions and Cross-sectional features

For the arch with variable cross-section, its geometric structure is shown in Figure 1, where S is the arc length, L is the span of the arch, R is the radius of the arch, f is the sagittal height of an arch, q is the locally uniformly distributed radial load, k is the stiffness of the arch end connection, 2Θ is the included angle of the arch, θ is the twist angle of the cross-section, c is the load area distribution angle, ϕ is the angular coordinates of the arch, u, v, and w are respectively the lateral displacement, radial displacement, and axial displacement.

Preprints (www.preprints.org) | NOT PEER-REVIEWED | Posted: 13 October 2023 doi:10.20944/preprints202310.0874.v1

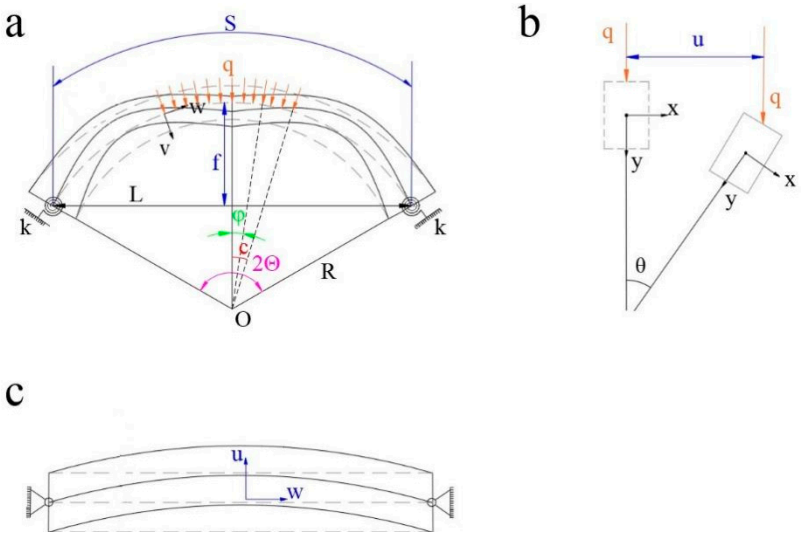

Figure 1. Geometric structure of variable cross-sectional arch: (a) Front view; (b) lateral view; (c) Flat view.

To facilitate the analysis of out-plane buckling in arches with variable cross-sections, the following fundamental assumptions are adopted in this study:

(1) The cross-section of the arch remains perpendicular to the arch axis throughout the buckling process.

(2) An exponential function with the base of the natural constant *e* is employed as the variable cross-sectional form.

(3)The span and height of the arch are significantly larger than the dimensions of the cross-section are assumed.

(4) The cross-section of the arch is assumed to be rectangular, exhibiting continuous and uniform variations along its length.

(5) The material of the arch is assumed to be uniform, isotropic, and exhibit linear elasticity. The elastic modulus is represented as *E*, and the shear modulus as *G*.

3. Analysis of variable cross-section

In previous out-plane buckling analysis of the arch[31,32] the cross-sectional height *h* is usually constant along the arch axis, and so the area *A*, the second moment of area *I*, the Saint–Venant torsional constant *J* and the warping constant I_w of the cross-section are also constant along the arch axis. In this paper, however, the cross-sectional height *h* varies continuously along the arch axis, the relevant cross-sectional parameters also vary, and *h* is defined by

$$h(\phi) = h_0 e^{a|\phi|} \tag{1}$$

with *a* being the variable cross-sectional index, which can be given by

$$a = \frac{\ln(h_e / h_0)}{\Theta} \tag{2}$$

where h_0 and h_e are the central and the end cross-sectional height, respectively. The average cross-sectional height hm can be obtained by integrating the cross-sectional height along the arch axis, as

Preprints (www.preprints.org) | NOT PEER-REVIEWED | Posted: 13 October 2023 doi:10.20944/preprints202310.0874.v1

$$h_m = \frac{\int_{-\Theta}^{\Theta} h(\phi)\,\mathrm{d}\phi}{\int_{-\Theta}^{\Theta} \mathrm{d}\phi} = \frac{h_0\left(e^{a\Theta}-1\right)}{a\Theta} \tag{3}$$

Thus, the corresponding average cross-sectional radius of rotation r_{xm} can be derived as

$$r_{xm} = \sqrt{\frac{1}{12}} h_m \tag{4}$$

For internal force analysis of variable cross-sectional arches, the calculation of the cross-sectional area A and the second moment of area about its major principal axis I_x are essential, and A and I_x are defined by

$$A(\phi) = \int_A \mathrm{d}\,A = b h_0 e^{a|\phi|} = A_0 e^{a|\phi|} \tag{5}$$

$$I_x(\phi) = \int_A y^2\,\mathrm{d}\,A = \frac{b h_0^3 e^{3a|\phi|}}{12} = I_{x0} e^{3a|\phi|} \tag{6}$$

For out-plane buckling of variable cross-sectional arches having rectangular thin-walled sections, the effects of the cross-sectional second moment of area about its minor principal axis I_y, the cross-sectional warping constant I_w and the cross-sectional Saint–Venant torsional constant J should be considered in the total potential during out-plane buckling, which can be defined by

$$r_{xm} = \sqrt{\frac{1}{12}} h_m \tag{7}$$

$$I_w(\phi) = \int_A \left[\omega(x,y)\right]^2 \mathrm{d}\,A = \frac{b^3 h_0^3 e^{3a|\phi|}}{144} = I_{w0} e^{3a|\phi|} \tag{8}$$

$$J(\phi) = \int_A \left[\left(x - \frac{\partial\omega(x,y)}{\partial x}\right)^2 + \left(y + \frac{\partial\omega(x,y)}{\partial y}\right)^2\right] \mathrm{d}\,A = \frac{b h_0 e^{a|\phi|}}{3} = J_0 e^{a|\phi|} \tag{9}$$

with the warping function being given by

$$\omega(x,y) = -xy \tag{10}$$

In addition, the shear correction coefficient of rectangular thin-walled section is not affected by the variation of cross-sectional height, which is a constant and can be expressed as

$$\mu_y(\phi) = \frac{5}{6} \tag{11}$$

Preprints (www.preprints.org) | NOT PEER-REVIEWED | Posted: 13 October 2023 doi:10.20944/preprints202310.0874.v1

4. Out-plane Buckling

4.1. Internal force and normal stress of variable cross-sectional arch

According to previous numerical analysis studies[28], reasonable variation of cross-sectional height of an arch can decrease its bending moment, and thus increase its critical load of out-plane buckling. It is also known [29, 30] that the accurate analytical solutions of internal forces and normal stress of a variable cross-sectional arch are indispensable for out-plane buckling analysis of the arch. These solutions can also be used to investigate the influences of the variable cross-section on the axial compression, bending moment and normal stress, which in turn affect the critical buckling load of out-plane buckling significantly. However, no analytical solutions of internal forces and normal stress of variable cross-sectional arches under a uniformly distributed radial local load are applicable in the opening literature. The analytical solutions of internal forces for a variable cross-sectional arch can be obtained using the Castigliano's second theorem.

The variable cross-sectional arch is a statically indeterminate structure. By cutting the crown of the variable cross-sectional arch into two parts, three redundant internal force, including central axial compression N_c, central bending moments M_c and central shear forces Q_{yc} are created on the crown, which is plotted in Figure 2a. For the principle of structural symmetry, the central shear force Q_{yc} should be equal to zero, so the mechanical model in Figure 2a can be simplified to that in Figure 2b. In addition, for equivalence of the cut arch to the original arch, the relative axial displacement ΔN_c and the relative rotation ΔM_c of the cut arch corresponding to central axial compression N_c and central bending moments M_c are also equal to zero, as

$$\Delta_{Nc} = 0 \quad \text{and} \quad \Delta_{Mc} = 0, \tag{12}$$

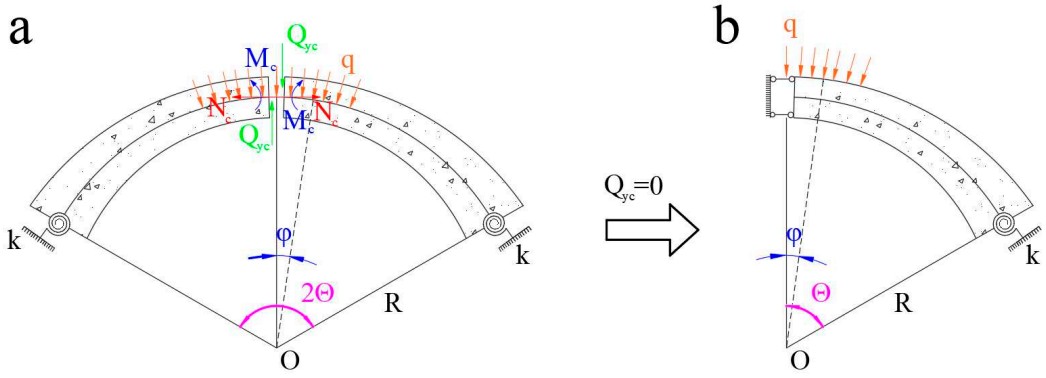

Figure 2. Basic system of variable cross-sectional arch.

According to Castigliano's second theorem, the relative axial displacement ΔN_c and the relative rotation ΔM_c can be also expressed as

$$\Delta_{Nc} = \frac{\partial U_{ss0}}{\partial N_c} = 0 \text{ and } \Delta_{Mc} = \frac{\partial U_{ss0}}{\partial M_c} = 0 \tag{13}$$

Where U_{ss0} is the pre-buckling total strain energy of the cut arch in Figure 2b, which is stated as

$$U_{ss0`} = \frac{1}{2}\int_0^{\Theta}\left[\frac{N(\phi)^2}{EA(\phi)} + \frac{M(\phi)^2}{EI_x(\phi)} + \frac{\beta Q_y(\phi)^2}{EA(\phi)}\right]R\mathrm{d}\phi + \frac{1}{2}\frac{M(\Theta)^2}{k(\Theta)} \tag{14}$$

where E is the modulus of elasticity, N is axial compression, M is bending moment, Q_y is shear force, k is the stiffness of the elastic rotation constraint, β is shear constant, and β can be denoted as

Preprints (www.preprints.org) | NOT PEER-REVIEWED | Posted: 13 October 2023 doi:10.20944/preprints202310.0874.v1

$$\beta = \frac{2(1+v_0)}{\mu_y} \tag{15}$$

With v_0 being the Poisson's ratio. The internal forces N, M and Q_y of the cut arch in Figure 3b can be obtained by static force equilibrium method, as

$$N = \begin{cases} N_c \cos\phi + qR(1-\cos c\cos\phi) & 0 \le \phi \le c \\ N_c \cos\phi + qR\sin c\sin\phi & c \le \phi \le \Theta \end{cases} \tag{16}$$

$$M = \begin{cases} M_c + N_c R(1-\cos\varphi) - qR^2(1-\cos c\cos\phi) & 0 \le \phi \le c \\ M_c + N_c R(1-\cos\varphi) - qR^2\sin c\sin\phi & c \le \phi \le \Theta \end{cases} \tag{17}$$

$$Q_y = \begin{cases} -N_c \sin\varphi + qR\sin\phi & 0 \le \phi \le c \\ -N_c \sin\varphi + qR\sin c\cos\phi & c \le \phi \le \Theta \end{cases} \tag{18}$$

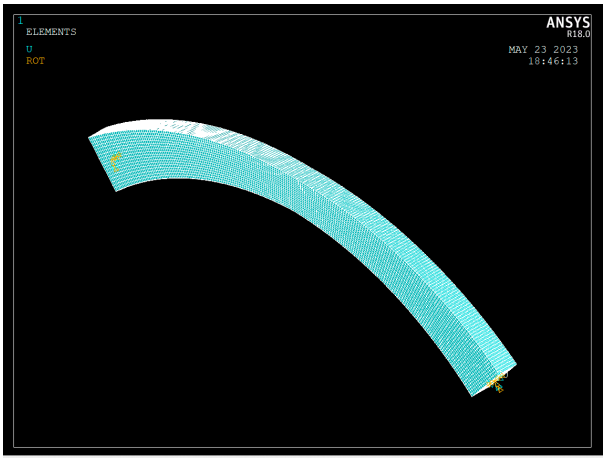

Figure 3. Variable cross-sectional arch model in ANSYS.

Substituting the strain energy obtained from Equation (14) into Equation (13), the force method equilibrium equations can then be given by

$$\int_0^{\Theta}\left[\frac{N(\phi)}{EA(\phi)}\frac{\partial N}{\partial M_c} + \frac{M(\phi)}{EI_x(\phi)}\frac{\partial M}{\partial M_c} + \frac{\beta Q_y(\phi)}{EA(\phi)}\frac{\partial Q_y}{\partial M_c}\right]R\mathrm{d}\phi + \frac{M(\Theta)}{k(\Theta)}\frac{\partial M(\Theta)}{\partial M_c} = 0 \tag{19}$$

$$\int_0^{\Theta}\left[\frac{N(\phi)}{EA(\phi)}\frac{\partial N}{\partial N_c} + \frac{M(\phi)}{EI_x(\phi)}\frac{\partial M}{\partial N_c} + \frac{\beta Q_y(\phi)}{EA(\phi)}\frac{\partial Q_y}{\partial N_c}\right]R\mathrm{d}\phi + \frac{M(\Theta)}{k(\Theta)}\frac{\partial M(\Theta)}{\partial N_c} = 0 \tag{20}$$

By substituting Equations (16), (17) and (18) into Equations (19) and (20), the linear homogeneous equations can be easily obtained, which can be expressed as

$$A_{11}M_c + A_{12}N_c + A_{13} = 0 \tag{21}$$

$$A_{21}M_c + A_{22}N_c + A_{23} = 0 \tag{22}$$

where the coefficients A_{11}, A_{12}, A_{13}, A_{21}, A_{22} and A_{23} are given in Appendix A. The central axial compression N_c and the central bending moment M_c can be obtained by solving the linear homogeneous Equations (21) and (22), as

Preprints (www.preprints.org) | NOT PEER-REVIEWED | Posted: 13 October 2023 doi:10.20944/preprints202310.0874.v1

$$N_c = \frac{A_{13}A_{21} - A_{11}A_{23}}{A_{11}A_{22} - A_{12}A_{21}} \tag{23}$$

$$M_c = \frac{A_{12}A_{23} - A_{13}A_{22}}{A_{11}A_{22} - A_{12}A_{21}} \tag{24}$$

Substituting two redundant internal forces N_c and M_c given by Equations (21) and (22) into Equations (16) and (17), the axial compression N and the bending moment M of the whole variable corss-sectional arch can then be expressed as

$$N = \begin{cases} qR\left(E_2\cos\phi - \sin c\sin\phi\right) & \Theta \le \phi \le -c \\ qR\left(E_2\cos\phi - \cos c\cos\phi + 1\right) & -c \le \phi \le c \\ qR\left(E_2\cos\phi + \sin c\sin\phi\right) & c \le \phi \le \Theta \end{cases} \tag{25}$$

$$M = \begin{cases} qR^2\left(E_1 - E_2\cos\varphi + \sin c\sin\phi\right) & \Theta \le \phi \le -c \\ qR^2\left(E_1 - E_2\cos\varphi + \cos c\cos\phi - 1\right) & -c \le \phi \le c \\ qR^2\left(E_1 - E_2\cos\varphi - \sin c\sin\phi\right) & c \le \phi \le \Theta \end{cases} \tag{26}$$

where non-dimensional parameters E_1 and E_2 can be given by

$$E_1 = \frac{M_c + N_c R}{qR^2} \text{ and } E_2 = \frac{N_c}{qR} \tag{27}$$

In addition, ε_{ss0} is pre-buckling normal strain, which can be stated as

$$\begin{aligned} \varepsilon_{ss0}(\phi) &= \frac{dw(\phi)}{d\phi} - \frac{v(\phi)}{R} - \frac{y}{R}\frac{\mathrm{d}\psi_y(\phi)}{\mathrm{d}\phi} \\ &= -\frac{N(\phi)}{EA(\phi)} + \frac{yM(\phi)}{EI(\phi)} \end{aligned} \tag{28}$$

According to Equations (25), (26) and (28), stresses of cross-sectional upper and lower edge fibres for a rectangular variable cross-sectional arch, which can be derived, respectively, as

$$\sigma_{su}(\phi) = -\frac{N(\phi)}{A(\phi)} - \frac{h_0 e^{a|\phi|}M(\phi)}{2I(\phi)} \tag{29}$$

$$\sigma_{sl}(\phi) = -\frac{N(\phi)}{A(\phi)} + \frac{h_0 e^{a|\phi|}M(\phi)}{2I(\phi)} \tag{30}$$

4.2. Critical out-plane buckling load of variable cross-sectional arch

For an arch with rectangular thin-walled sections, where the cross-sectional height is much larger than the cross-sectional width, it is well known that when the internal forces induced by external loads in a variable cross-sectional arch reach a critical value, the arch may experience out-plane buckling. Therefore, the variation in cross-sectional height directly affects the internal forces within the arch, which in turn has a significant impact on the critical load for out-plane buckling. Additionally, based on previous research on the analysis of out-plane buckling in arches[33], the total potential energy of the variable cross-sectional arch during out-plane buckling can be expressed as

Preprints (www.preprints.org) | NOT PEER-REVIEWED | Posted: 13 October 2023 doi:10.20944/preprints202310.0874.v1

$$\Pi=\int_{-\Theta}^{\Theta}\left\{\frac{EI_y(\phi)}{2R}\left(\theta+\tilde{u}''\right)^2+\frac{GJ(\phi)}{2R}\left(\theta'-\tilde{u}'\right)^2+\frac{EI_w(\phi)}{2R^3}\left(\theta''-\tilde{u}''\right)^2\right\}\mathrm{d}\phi$$
$$+\int_{-\Theta}^{\Theta}\left\{M(\phi)\left(\tilde{u}''\theta+\frac{\theta^2}{2}+\frac{\tilde{u}'^2}{2}\right)-N(\phi)R\left[\frac{\tilde{u}'^2}{2}+\frac{r_0^2(\phi)}{2R^2}\left(\theta'-\tilde{u}'\right)^2\right]\right\}\mathrm{d}\phi \tag{31}$$

Where

$$r_0(\phi)=\sqrt{\frac{I_x(\phi)+I_y(\phi)}{A(\phi)}}=\sqrt{\left(\frac{1}{12}h_0^2\right)e^{2a|\phi|}+\left(\frac{1}{12}b^2\right)}=\sqrt{r_{x0}^2e^{2a|\phi|}+r_y^2} \tag{32}$$

with r_{x0} is the in-plane gyration radius of central cross-section and r_y is out-plane gyration radius.

For determine the critical buckling load of out-plane buckling for variable cross-sectional arches subjected to a uniformly distributed radial local load, the required equilibrium differential equation can be derived by the Ritz method.

According to the above, the lateral displacement $\tilde{u}(\phi)$, torsional angle $\theta(\phi)$ can be assumed respectively as

$$\tilde{u}(\phi)=\tilde{u}_1\cos\frac{\pi\phi}{2\Theta} \tag{33}$$

$$\theta(\phi)=\theta_1\cos\frac{\pi\phi}{2\Theta} \tag{34}$$

Substituting Equations (33)-(34) into the total potential energy of the variable cross-sectional arch during out-plane buckling obtained from Equation (31), the Equation (31) can be rewritten as

$$\Pi=\frac{1}{2}\left\{\tilde{u}_1\quad\theta_1\right\}\left(\boldsymbol{K}_e+qR\boldsymbol{K}_g\right)\begin{Bmatrix}\tilde{u}_1\\ \theta_1\end{Bmatrix} \tag{35}$$

where the stiffness matrixes K_e and K_g can be respectively expressed as

$$\boldsymbol{K}_e=\begin{bmatrix}k_{e11} & k_{e12}\\ k_{e12} & k_{e22}\end{bmatrix} \tag{36}$$

$$\boldsymbol{K}_g=\begin{bmatrix}k_{g11} & k_{g12}\\ k_{g12} & k_{g22}\end{bmatrix} \tag{37}$$

with the elements of the stiffness matrixes K_e and K_g being given by

$$k_{e11}=\frac{EI_{w0}\pi^4\left(\pi^2e^{3a\Theta}-18\Theta^2a^2-\pi^2\right)}{48R^3\Theta^4a\left(9\Theta^2a^2+\pi^2\right)}-\frac{EI_{y0}\pi^4\left(2\Theta^2a^2-e^{a\Theta}\pi^2+\pi^2\right)}{16R\Theta^4a\left(\Theta^2a^2+\pi^2\right)}$$
$$+\frac{GJ_0\pi^2\left(2e^{a\Theta}\Theta^2a^2+e^{a\Theta}\pi^2-\pi^2\right)}{4R\Theta^2a\left(\Theta^2a^2+\pi^2\right)} \tag{38}$$

Preprints (www.preprints.org) | NOT PEER-REVIEWED | Posted: 13 October 2023 doi:10.20944/preprints202310.0874.v1

$$k_{e12}=\frac{EI_{y0}\pi^2\left(2\Theta^2a^2-\mathrm{e}^{a\Theta}\pi^2+\pi^2\right)}{4R\Theta^2a\left(\Theta^2a^2+\pi^2\right)}-\frac{EI_{w0}\pi^4\left(\pi^2\mathrm{e}^{3a\Theta}-18\Theta^2a^2-\pi^2\right)}{48R^3\Theta^4a\left(9\Theta^2a^2+\pi^2\right)}-\frac{GJ_0\pi^2\left(2\mathrm{e}^{a\Theta}\Theta^2a^2+\mathrm{e}^{a\Theta}\pi^2-\pi^2\right)}{4R\Theta^2a\left(\Theta^2a^2+\pi^2\right)} \tag{39}$$

$$k_{e22}=\frac{EI_{y}\pi^2\left(2\Theta^2a^2-\mathrm{e}^{a\Theta}\pi^2+\pi^2\right)}{4R\Theta^2a\left(\Theta^2a^2+\pi^2\right)}-\frac{EI_{w}\pi^4\left(\pi^2\mathrm{e}^{3a\Theta}-18\Theta^2a^2-\pi^2\right)}{48R^3\Theta^4a\left(9\Theta^2a^2+\pi^2\right)}-\frac{GJ\pi^2\left(2\mathrm{e}^{a\Theta}\Theta^2a^2+\mathrm{e}^{a\Theta}\pi^2-\pi^2\right)}{4R\Theta^2a\left(\Theta^2a^2+\pi^2\right)} \tag{40}$$

$$k_{g11}=\frac{\pi\left(2R^2+r_y^2\right)}{4\Theta^2R}\left[\pi(\pi^2-2\Theta^2)F_1-F_2-\pi c\right]+\frac{E_1\pi^2R}{4\Theta}+\frac{\pi^2r_{x0}^2\chi}{R} \tag{41}$$

$$k_{g12}=\frac{\pi^2\left[\pi^2(R^2+r_y^2)-2\Theta^2r_y^2\right]F_1-\pi(R^2-r_y^2)F_2}{4\Theta^2R}+\frac{\pi^2c(R^2+r_0^2)}{4\Theta^2R}-\frac{\pi^2E_1R}{4\Theta}-\frac{\pi^2r_{x0}^2\chi}{R} \tag{42}$$

and

$$k_{g22}=\frac{\pi^2F_1\left[\pi^2r_0^2+2\Theta^2(2R^2-r_y^2)\right]}{4\Theta^2R}-\frac{c(\pi^2r_y^2+4R^2\Theta^2)}{4R\Theta^2}+E_1\Theta R+\frac{F_2(4R^2\Theta^2-\pi^2r_y^2)}{4\Theta^2R\pi}+\frac{\pi^2r_{x0}^2\chi}{R} \tag{43}$$

in which the parameters F_1, F_2 and χ are given by

$$F_1=\frac{sin\,c\,cos\,\Theta-E_2\,sin\,\Theta}{\pi^2-\Theta^2},\quad F_2=\frac{\Theta^3\,sin\left(\frac{c\pi}{\Theta}\right)}{\pi^2-\Theta^2} \tag{44}$$

and

Preprints (www.preprints.org) | NOT PEER-REVIEWED | Posted: 13 October 2023 doi:10.20944/preprints202310.0874.v1

$$\begin{aligned}\chi=&\frac{1}{2\Theta^2\left(4a^2+1\right)}\left[\frac{\pi^2 a\left(E_2-\cos c\right)\left(4\Theta^2a^2+\pi^2-3\Theta^2\right)}{\left(4a^2+1\right)^2\Theta^4+\pi^4+2\pi^2\Theta^2\left(4a^2-1\right)}-\frac{e^{2ca}}{4a}\right]\\&+\frac{\Theta e^{2ca}}{2}\frac{2\Theta a\left[\left(4a^2+1\right)\Theta^2-3\pi^2\right]\cos\left(\frac{c\pi}{\Theta}\right)+\pi\left[\left(12a^2+1\right)\Theta^2-\pi^2\right]\sin\left(\frac{c\pi}{\Theta}\right)}{3\Theta^6a^2\left(4a^2+1\right)^2+2\pi^2\Theta^4\left(48a^4+1\right)+4\pi^4\Theta^2\left(6a^2-1\right)+2\pi^6}\\&-\frac{e^{2ca}\left(E_2\sin\Theta-\cos\Theta\sin c\right)\left[2\left(4a^2+1\right)^2\Theta^4+\left(4a^2-3\right)\pi^2\Theta^2+\pi^4\right]}{4\Theta^2\left(4a^2+1\right)\left[\Theta^4\left(4a^2+1\right)^2+2\pi^2\Theta^2\left(4a^2-1\right)+\pi^4\right]}\\&-\frac{e^{2ca}a\left(E_2\cos\Theta+\sin\Theta\sin c\right)\left[2\Theta^4\left(4a^2+1\right)^2+\pi^2\Theta^2\left(12a^2-1\right)+\pi^4\right]}{2\Theta^2\left(4a^2+1\right)\left[\Theta^4\left(4a^2+1\right)^2+2\pi^2\Theta^2\left(4a^2-1\right)+\pi^4\right]}\\&+\frac{\pi^2}{8\Theta^2a\left(4\Theta^2a^2+\pi^2\right)}\end{aligned}\tag{45}$$

In order to minimize the total potential energy of the variable cross-sectional arch during out-plane buckling, the principle of Rayleigh-Ritz method can be used, the constraint conditions of the cross-sectional lateral displacement $\tilde{u}(\phi)$ and torsional angle $\theta(\phi)$ of the arch are obtained as

$$\begin{cases}\dfrac{\partial\Pi(\tilde{u}_1,\theta_1)}{\partial\tilde{u}_1}=\left(k_{e11}+\dfrac{Q_{cr}}{N_y}k_{h11}\right)\tilde{u}_1+\left(k_{e12}+\dfrac{Q_{cr}}{N_y}k_{h12}\right)\theta_1=0\\[2ex]\dfrac{\partial\Pi(\tilde{u}_1,\theta_1)}{\partial\theta_1}=\left(k_{e12}+\dfrac{Q_{cr}}{N_y}k_{h12}\right)\tilde{u}_1+\left(k_{e22}+\dfrac{Q_{cr}}{N_y}k_{h22}\right)\theta_1=0\end{cases}\tag{46}$$

where Q_{cr} is the critical out-plane buckling load of the variable cross-sectional arch under a uniformly distributed radial local load, which can be express as

$$Q_{cr}=2cRq_{cr}\tag{47}$$

N_y is the critical buckling load of the simply supported column having the cross-sectional height h_0 and the length S, which can be given by

$$N_y=\frac{\pi^2EI_{y0}}{S^2}\tag{48}$$

k_{h11}, k_{h12} and k_{h22} is the elements of the stiffness matrixes K_h, and the stiffness matrixes K_h can be stated as

$$\boldsymbol{K_h}=\frac{N_y}{2c}\boldsymbol{K_g}\tag{49}$$

The Equation (46) can be rewritten into a displacement vector-stiffness matrix form, as

$$\boldsymbol{K}\begin{Bmatrix}\tilde{u}_1\\\theta_1\end{Bmatrix}=\left(\boldsymbol{K_e}+\frac{Q_{cr}}{N_y}\boldsymbol{K_h}\right)\begin{Bmatrix}\tilde{u}_1\\\theta_1\end{Bmatrix}=0\tag{50}$$

Let the determinant of the stiffness matrix K obtained from Equation (50) equal to zero, as

Preprints (www.preprints.org) | NOT PEER-REVIEWED | Posted: 13 October 2023 doi:10.20944/preprints202310.0874.v1

$$\left(k_{h11}k_{h22}-k_{h12}^2\right)\left(\frac{Q_{cr}}{N_y}\right)^2+\left(k_{e11}k_{h22}-2k_{e12}k_{h12}+k_{e22}k_{h11}\right)\frac{Q_{cr}}{N_y}+k_{e11}k_{e22}-k_{e12}^2=0 \quad (51)$$

The non-dimensional critical buckling load Q_{cr}/N_y can be obtained by solving the quadratic equation obtained from Equation (51).

5. Comparisons with Finite Element (FE) Results

5.1. Numerical model of the arch with variable cross-section

According to the Timoshenko beam theory, the beam 188 element of ANSYS is suitable for constructing a variable cross-sectional arch model that considers shear deformation. Hence, the results obtained from ANSYS for variable cross-sectional arches with different cross-sectional indexes and included angles are compared against the analytical solution provided by Equation (51). This comparison aims to verify whether the non-dimensional critical out-plane buckling load Q_{cr}/N_y, obtained from Equation (51), can accurately predict out-plane buckling behaviour of variable cross-sectional arches subjected to a uniformly distributed radial local load.

In the variable cross-sectional arch model shown in Figure 3, the material's Young's modulus E is 34.5GPa, the cross-sectional width b is 0.15m, the average cross-sectional height h_m is 0.25m, the in-plane slenderness ratio S/r_{xm} is 50, and the out-plane slenderness ratio S/r_y is 83.3. Additionally, the variable cross-sectional arch models have in-plane elastic rotation constraints and are subjected to a uniformly distributed radial local load. The flexibility coefficient of the elastic rotation constraint is ζ=0.1, and the ratio of the action length of the local load is c/Θ=0.5.

5.2. Comparative analysis with finite element results

The comparisons of internal forces of the variable cross-sectional arches between the analytical solutions obtained from Equations (25) and (26) and the ANSYS results are plotted in Figure 4a as the curves of the non-dimensional central axial compression N_c/Q with included angle 2Θ and in Figure 4b as the curves of the non-dimensional central bending moment $4M_c/QL$ with included angle 2Θ for variable cross-sectional arches having different cross-sectional height ratio h_e/h_0, where he and h_0 are the end and central cross-sectional height, respectively, and $Q = 2qcR$.

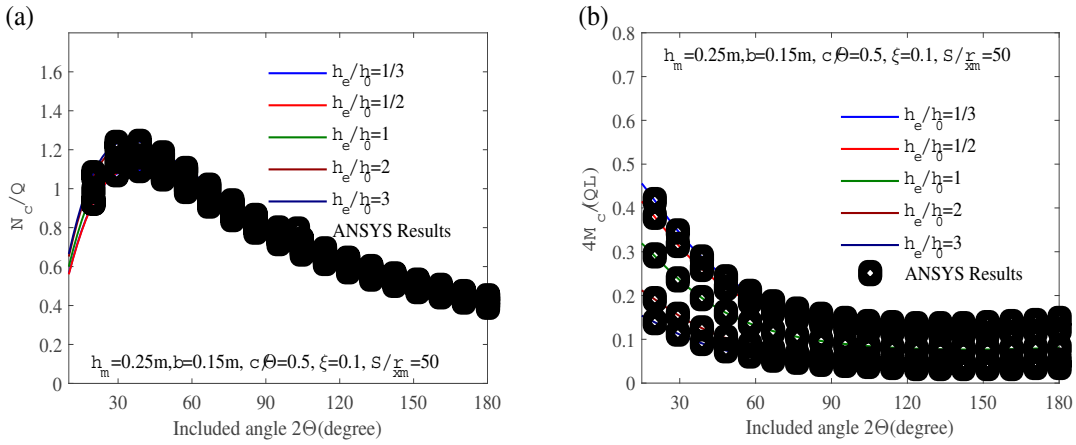

Figure 4. Analytical solution of internal force: (a) axial compression N_c/Q; (b)bending moment $4M_c/(QL)$.

It can be seen from Figure 4a and 4b that the analytical solutions of the axial compressions and bending moments obtained from Equations (25) and (26) agree excellently against the ANSYS results,

Preprints (www.preprints.org) | NOT PEER-REVIEWED | Posted: 13 October 2023 doi:10.20944/preprints202310.0874.v1

so the solutions obtained from Equations (25) and (26) can predict the internal forces of variable cross-sectional arches under a uniformly distributed radial local load.

In addition, it can be indicated from Figure 4a that variations of axial compression of variable cross-sectional arches with the included angle are similar to those of uniform cross-sectional arches. When the included angle 2Θ increase, the non-dimensional central axial compression increases significantly at first, and then slightly decreases. However, for the same volume of variable cross-sectional arches and uniform cross-sectional arches, when the cross-sectional height ratio h_e/h_0 increases, the non-dimensional central axial compression increases. It can be indicated from Figure 4b that variations of bending moment of variable cross-sectional arches with the included angle are similar to those of uniform cross-sectional arches. When the included angle 2Θ increase, the non-dimensional central bending moment decreases significantly at first, and then slightly increases. However, for the same volume of variable cross-sectional arches and uniform cross-sectional arches, when the cross-sectional height ratio he/h0 increases, the non-dimensional central bending decreases.

The comparisons of critical out-plane buckling loads of the variable cross-sectional arches between the analytical solutions obtained from Equation (51) and the ANSYS results are plotted in Figure 5 as the curves of the non-dimensional critical out-plane buckling load Q_{cr}/N_y with included angle 2Θ for variable cross-sectional arches having different cross-sectional height ratio h_e/h_0.

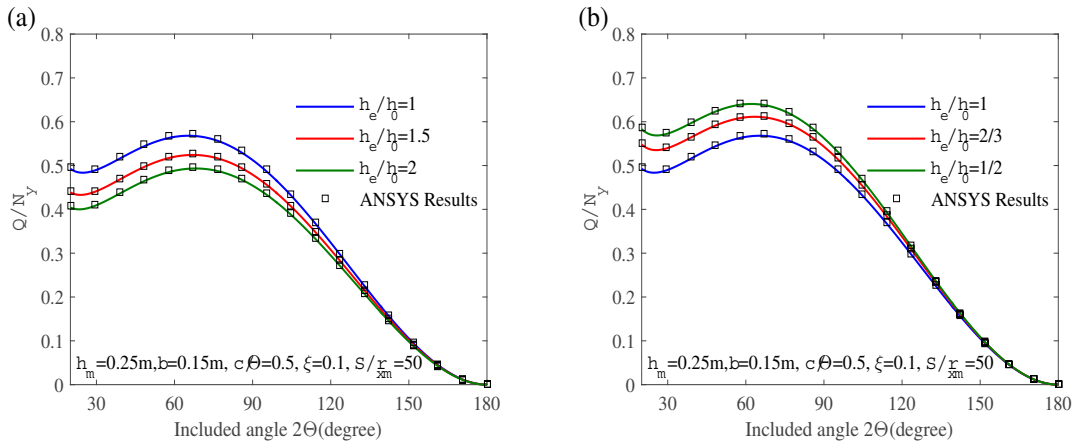

Figure 5. Analytical solution and finite element results of vault: （a）Included Angle; (b)Flexibility parameter.

It can be seen from Figure 5 that the analytical solutions of the critical out-plane buckling load obtained from Equation (51) agree excellently against the ANSYS results. Therefore, the solutions obtained from Equation (51) can predict the critical out-plane buckling loads of variable cross-sectional arches under a uniformly distributed radial local load.

In addition, for the same volume of variable cross-sectional arches and uniform cross-sectional arches, Figure 5 shows that when the cross-sectional height ratio h_e/h_0 increases, the non-dimensional critical out-plane buckling load increases.

6. Parametric analysis

6.1. Parametric analysis of Stresses and Internal Forces

The pre-buckling axial compression and bending moment behaviour and effects of cross-sectional height ratio h_e/h_0, in-plane slenderness ratio S/r_{xm}, flexibility coefficient of elastic rotation constraint ζ and ratio of action length of local load on the internal forces of variable cross-sectional arches are based on the analytical solutions obtained from Equations. (25)~(26), while the pre-buckling stresses behaviour of variable cross-sectional arches is based on the analytical solutions obtained from Equations (29)~(30).

Preprints (www.preprints.org) | NOT PEER-REVIEWED | Posted: 13 October 2023 doi:10.20944/preprints202310.0874.v1

To demonstrate the influence of the cross-sectional height ratio h_e/h_0 on pre-buckling stresses, distributions of stresses for variable cross-sectional arches with different cross-sectional height ratios (i.e., h_e/h_0 = 0.5, 1, and 2) are plotted in Figure 6a and 6b. The figures depict distributions of the stresses in the cross-sectional lower and upper edge fibers (i.e., σ_{sl} and σ_{su}) against the non-dimensional angular coordinates of the cross-section ϕ/Θ for shallow variable cross-sectional arches with an included angle of 2Θ=40°, respectively. Similarly, distributions of σ_{sl} and σ_{su} against ϕ/Θ are shown in Figure 6c and 6d for deep variable cross-sectional arches with an included angle of 2Θ=120°.

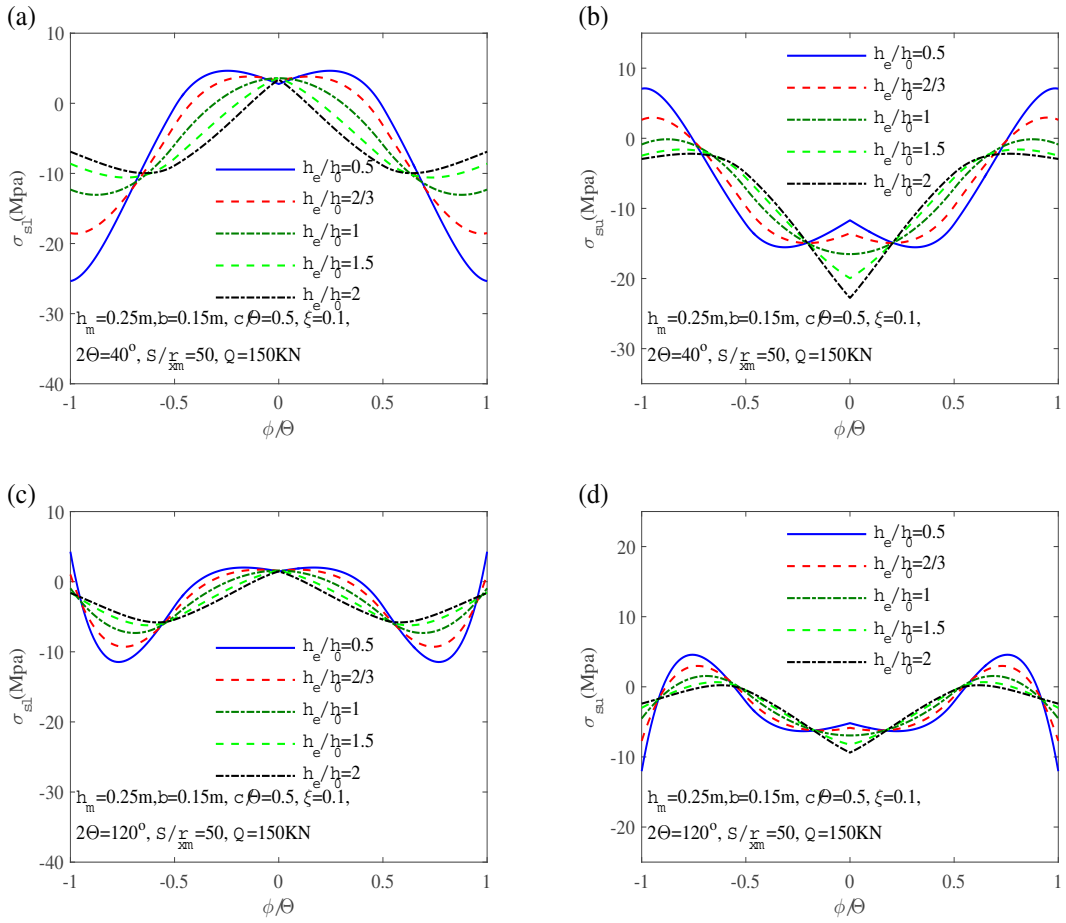

Figure 6. Distributions of the stresses in the cross-sectional lower edge fibers σ_{sl} and upper edge fibers σ_{su} along arch length: (a) Lower edge fibers σsl for shallow arch, 2Θ = 40º; (b) Upper edge fibers σsu for shallow arch, 2Θ = 40º; (c) Lower edge fibers σsl for deep arch, 2Θ = 120º; (d) Upper edge fibers σsu for deep arch, 2Θ = 120º.

Figure 6 demonstrates that as the cross-sectional height ratio of the variable cross-sectional arch increases, the stress distribution in the arch becomes more uniform. In addition, for shallow variable cross-sectional arches, Figure 6a and 6b indicated that the stresses at the upper and lower edges of the cross-section are primarily compressive. However, there may be instances of tensile stresses present at the upper edge of the cross-section in the end support segments, as well as at the lower edge of the cross-section in the crown segments. As the cross-sectional height ratio of the variable cross-sectional arch increases, the segment of the arch axis experiencing tensile stresses gradually decreases. Therefore, designing variable cross-sectional arches with a larger cross-sectional height ratio is advantageous for structures with lower tensile strength, such as reinforced concrete structures. For deep variable cross-sectional arches, Figure 6c and 6d indicated that the upper and lower edges of the cross-section also primarily experience compressive stresses. However, apart from the potential occurrence of tensile stresses at the lower edge of the cross-section in the end support segments and at the lower edge of the cross-section in the crown segments, there might also be

Preprints (www.preprints.org) | NOT PEER-REVIEWED | Posted: 13 October 2023 doi:10.20944/preprints202310.0874.v1

instances of tensile stresses at the upper edge of the cross-section near the end support segments. This phenomenon arises from the presence of inflection points in the end support segments of the arch. As the cross-sectional height ratio h_e/h_0 of the variable cross-sectional arch increases, the segments of the arch axis experiencing tensile stresses also gradually decrease.

To demonstrate the effects of cross-sectional height ratio h_e/h_0 and in-plane slenderness ratio S/r_{xm} on the pre-buckling internal force, the analytical solutions of internal forces of variable cross-sectional arches having different cross-sectional height ratio (i,e,. h_e/h_0 = 0.5, 1 and 2) are plotted in Figure 7a as the curves of the non-dimensional central axial compression N_c/Q versus in-plane slenderness ratio S/r_{xm} for shallow variable cross-sectional arches having a included angle 2Θ=40°, in Figure 7b as the curves of the non-dimensional central bending moment $4M_c/QL$ versus in-plane slenderness ratio S/r_{xm} for shallow variable cross-sectional arches having a included angle 2Θ=40°, in Figure 7c as the curves of N_c/Q versus S/r_{xm} for deep variable cross-sectional arches having a included angle 2Θ=120°, in Figure 7d as the curves of $4M_c/QL$ versus S/rxm for deep variable cross-sectional arches having a included angle 2Θ=120°.

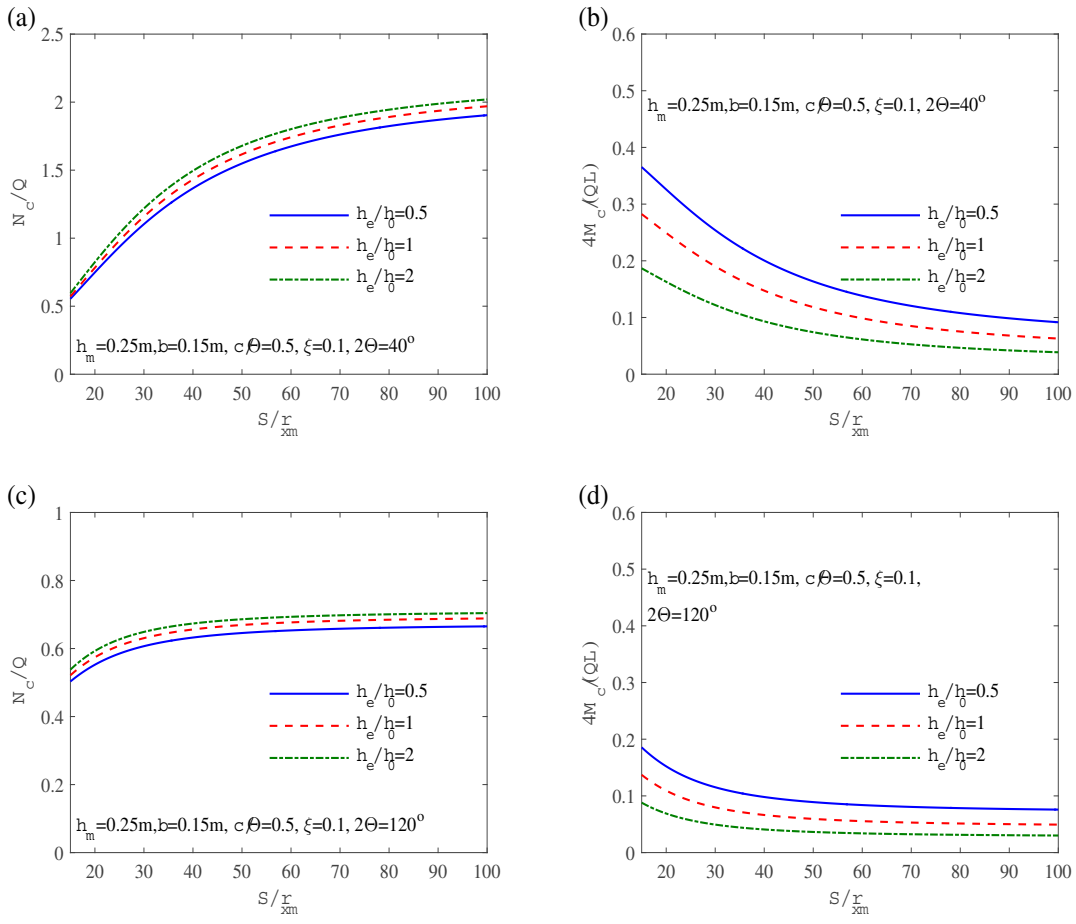

Figure 7. Influence of slenderness ratio S/rxm on the forces in the arch with variable cross-section: (a) Axial compression for $2\Theta = 40^{o}$; (b) Bending moment for $2\Theta = 40^{o}$; (c) Axial compression for $2\Theta = 120^{o}$; (d) Bending moment for $2\Theta = 120^{o}$.

Figures 7a and 7b demonstrate the variations in internal forces for shallow variable cross-sectional arches under slenderness ratio S/r_{xm}. Figure 7a shows that as the slenderness ratio S/r_{xm} increases, the axial compression N_c/Q in the shallow variable cross-sectional arch also increases. Figure 7b indicates that as the slenderness ratio S/r_{xm} increases, the bending moment $4M_c/QL$ in the shallow arch gradually decreases. Additionally, as the cross-sectional height ratio h_e/h_0 of the variable cross-sectional arch increases, larger axial compressions N_c/Q and smaller bending moments $4M_c/QL$ can be achieved, contributing to the compressive performance of the arch structure. Figures 7c and

Preprints (www.preprints.org) | NOT PEER-REVIEWED | Posted: 13 October 2023 doi:10.20944/preprints202310.0874.v1

7d demonstrate the variations in internal forces for deep variable cross-sectional arches under slenderness ratio S/r_{xm}. Both figure 7c and 7d lead to similar conclusions as shallow variable cross-sectional arches, where an increase in slenderness ratio S/r_{xm} corresponds to an increase in axial compression N_c/Q and a decrease in bending moment $4M_c/QL$ for deep variable cross-sectional arches. Similarly, with an increase in the cross-sectional height ratio h_e/h_0 of the variable cross-sectional arch, greater axial compressions and smaller bending moments $4M_c/QL$ can be obtained for deep variable cross-sectional arches as well. Furthermore, it is noticeable that shallow variable cross-sectional arches exhibit more pronounced changes in internal forces than those for deep variable cross-sectional arches in response to variations in the cross-sectional height ratio h_e/h_0 of the variable cross-sectional arch.

To explore the distribution law of internal force along the arch length, the distribution of non-dimensional axial compression N/Q and non-dimensional central bending moment $4M_c/(QL)$ along the length of variable section arch under a localized uniform radial load is shown in Figure 8. Figure 8a, Figure 8b, Figure 8c, and Figure 8d have the same parameters, mainly including the average cross-sectional height h_m=0.25m, cross-section width b=0.15m, the ratio of the action length c/Θ=0.5, the end rotation constraint ζ=0.1 and the slenderness ratio S/r_{xm}=50. Meanwhile, the included angle of Figure 8a and Figure 8b is 40º, the included angle of Figure 8c and Figure 8d is 120º.

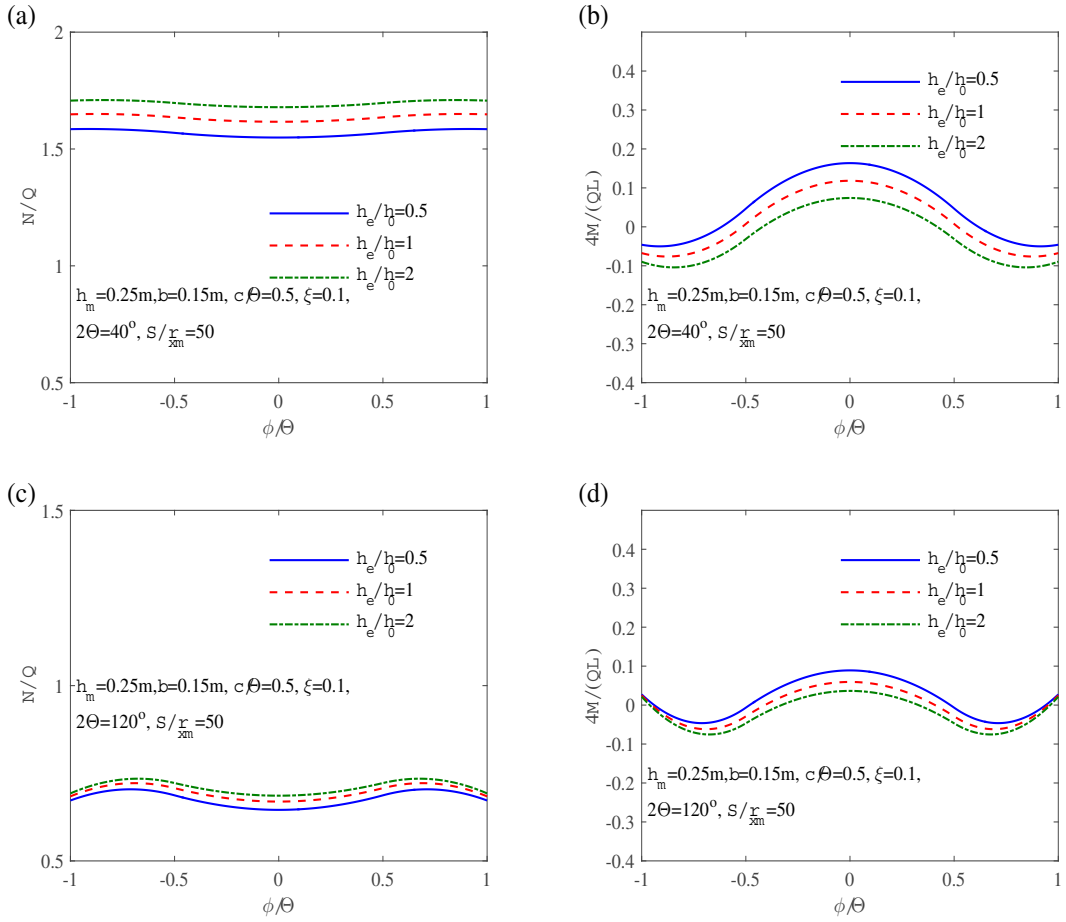

Figure 8. Distributions non-dimensional axial compression of N/Q and non-dimensional bending moment of $4M/QL$ along arch length: (a) Axial compression for 2Θ = 40º; (b) Bending moment for 2Θ = 40º; (c) Axial compression for 2Θ = 120º; (d) Bending moment 2Θ = 120º.

It can be seen from Figure 8 that for variable cross-sectional arch, the non-dimensional axial compression N/Q and non-dimensional central bending moment $4M_c/(QL)$ along the arch length is nonuniform. From Figures 8a and 8b, it can be observed that for shallow variable cross-sectional arches with 2Θ = 40º, the axial compression N/Q gradually increases as the cross-sectional height ratio

Preprints (www.preprints.org) | NOT PEER-REVIEWED | Posted: 13 October 2023 doi:10.20944/preprints202310.0874.v1

h_e/h_0 of the variable cross-sectional arch increases, while the bending moment $4M_c/(QL)$ decreases. Similarly, Figures 8c and 8d show that for deep variable cross-sectional arches with $2\Theta = 120^o$, the variations in axial compression N/Q and bending moment $4M_c/(QL)$ follow the same trend as in shallow variable cross-sectional arches, namely, an increase in the cross-sectional height ratio h_e/h_0 leads to an increase in axial compression N/Q and a decrease in bending moment $4M_c/(QL)$. Additionally, it should be noted that the effects of the cross-sectional height ratio h_e/h_0 on internal forces of shallow variable cross-sectional arches are more significant than those effects on deep variable cross-sectional arches.

To demonstrate the effects of cross-sectional height ratio h_e/h_0 and localized parameter c/Θ on the pre-buckling internal force, the analytical solutions of internal forces of variable cross-sectional arches having different cross-sectional height ratio (i,e,. $h_e/h_0 = 0.5$, 1 and 2) are plotted in Figure 9a as the curves of the non-dimensional central axial compression N_c/Q versus localized parameter c/Θ for shallow variable cross-sectional arches having a included angle 2Θ=40°, in Figure 9b as the curves of the non-dimensional central bending moment $4M_c/QL$ versus localized parameter c/Θ for shallow variable cross-sectional arches having a included angle 2Θ=40°, in Figure 9c as the curves of N_c/Q versus c/Θ for deep variable cross-sectional arches having a included angle 2Θ=120°, in Figure 9d as the curves of $4M_c/QL$ versus c/Θ for deep variable cross-sectional arches having a included angle 2Θ=120°.

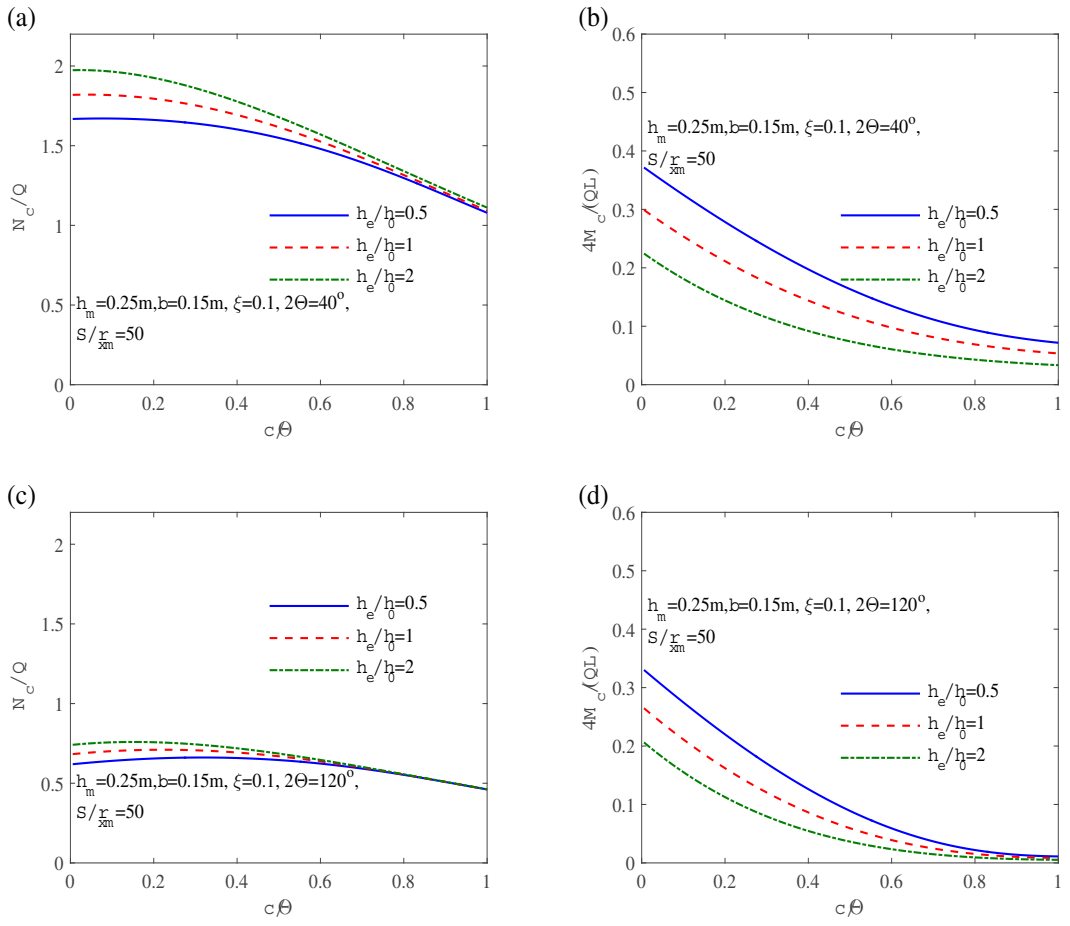

Figure 9. Influence of the localized parameter c/Θ on the forces in the arch with variable cross-section: (a) Axial compression for $2\Theta = 40^o$; (b) Bending moment for $2\Theta = 40^o$; (c) Axial compression for $2\Theta = 120^o$; (d) Bending moment for $2\Theta = 120^o$.

Figure 9a illustrates that as the ratio of the action length c/Θ increases, the axial compression of the arch with different cross-sectional height ratios h_e/h_0 gradually decreases, while the axial compression increases as the cross-sectional height ratio of the variable cross-sectional arch increases.

Preprints (www.preprints.org) | NOT PEER-REVIEWED | Posted: 13 October 2023 doi:10.20944/preprints202310.0874.v1

In Figure 9c, it can be observed that for the deep arch with 2Θ=120º, the change in the ratio of the action length c/Θ has little impact on the axial compression of the arch with different cross-sectional height ratios h_e/h_0. When the ratio of the action length c/Θ exceeds 0.6, the axial compression N/Q is nearly unaffected by the cross-sectional height ratio h_e/h_0. Moreover, Figures 9b and 9d reveal that as the ratio of the action length c/Θ increases, the bending moment of the arch with different cross-sectional height ratios h_e/h_0 gradually decreases, and the bending moment increases as the cross-sectional height ratio h_e/h_0 of the variable cross-sectional arch decreases.

To explore the effects of cross-sectional height ratio h_e/h_0 and the non-dimensional flexibility of the flexibility coefficient of elastic rotation constraint ζ on the pre-buckling internal force, the analytical solutions of internal forces of variable cross-sectional arches having different cross-sectional height ratio (i,e,. h_e/h_0 = 0.5, 1 and 2) are plotted in Figure 10a as the curves of the non-dimensional central axial compression N_c/Q versus ζ for shallow variable cross-sectional arches having a included angle 2Θ=40°, in Figure 10b as the curves of the non-dimensional central bending moment $4M_c/QL$ versus ζ for shallow variable cross-sectional arches having a included angle 2Θ=40°, in Figure 10c as the curves of N_c/Q versus ζ for deep variable cross-sectional arches having a included angle 2Θ=120°, in Figure 10d as the curves of $4M_c/QL$ versus ζ for deep variable cross-sectional arches having a included angle 2Θ=120°.

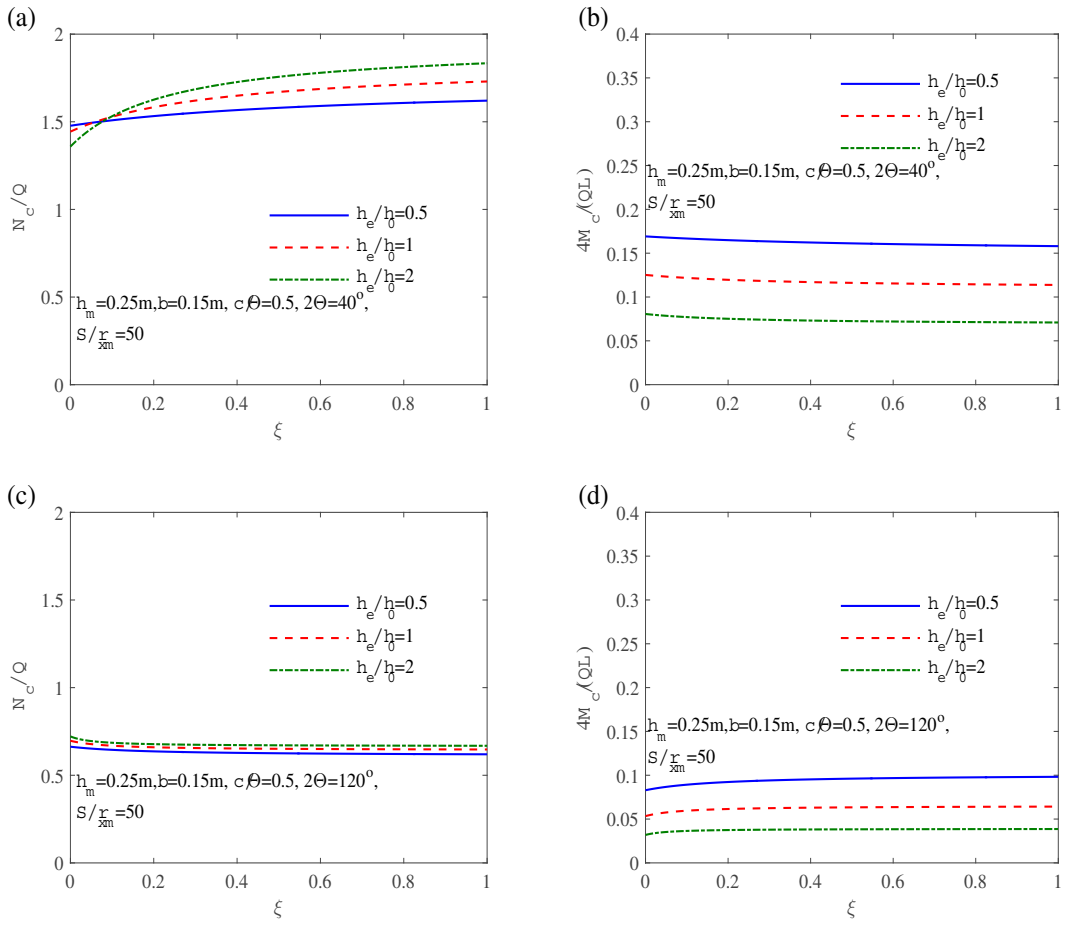

Figure 10. Influence of the non-dimensional flexibility of the flexibility coefficient of elastic rotation constraint ζ on the internal forces: (a) Axial compression for 2Θ = 40º; (b) Bending moment for 2Θ = 40º; (c) Axial compression for 2Θ = 120º; (d) Bending moment for 2Θ = 120º.

Figure 10a and Figure 10b illustrate the variations of axial compression N_c/Q and bending moment $4M_c/QL$ for shallow variable cross-sectional arches with different cross-sectional height ratio h_e/h_0 as the flexibility coefficient of elastic rotation constraint ζ change. According to Figure 10a, it can be observed that as the cross-sectional height ratio he/h0 increases, the axial compression N_c/Q of the

Preprints (www.preprints.org) | NOT PEER-REVIEWED | Posted: 13 October 2023 doi:10.20944/preprints202310.0874.v1

shallow variable cross-sectional arch gradually increases. Furthermore, the axial compression N_c/Q of the arch also increases with an increase in the flexibility coefficient of elastic rotation constraint ζ, and the rate of increase is higher for arches with larger cross-sectional height ratio h_e/h_0. From Figure 10b, it can be seen that as the cross-sectional height ratio h_e/h_0 increases, the bending moment $4M_c/QL$ of the shallow variable cross-sectional arch slightly decreases. The bending moment $4M_c/QL$ of the arch decreases with an increase in the flexibility coefficient of elastic rotation constraint ζ, but the decrease is not significant. Figures 10c and 10d represent the variations in axial compression N_c/Q and bending moment $4M_c/QL$ of deep variable cross-sectional arches with different cross-sectional height ratio h_e/h_0 under changing flexibility coefficient of elastic rotation constraint ζ. From Figure 10c, it can be observed that as the cross-sectional height ratio h_e/h_0 increases, the axial compression N_c/Q of deep variable cross-sectional arches slightly increases. Additionally, the axial compression decreases slightly with an increase in the end rotational restraint ζ. Figure 10d indicates that as the cross-sectional height ratio h_e/h_0 increases, the bending moment $4M_c/QL$ of shallow variable cross-sectional arches decreases to some extent. Moreover, with an increase in the end rotational restraint ζ, the bending moment $4M_c/QL$ of the arch increases, but the change is not significant.

According to Figures 7 to 10, it can be seen that compared with an arch with a uniform cross-section height ratio of h_e/h_0=1, for a variable cross-section arch with h_e/h_0 greater than 1, the axial compression N_c/Q of the arch is larger and the bending moment $4M_c/QL$ is smaller. However, for a variable cross-section arch with h_e/h_0 less than 1, the axial compression N_c/Q is smaller and the bending moment $4M_c/QL$ is larger. Therefore, the design of an arch with h_e/h_0 greater than 1 is more reasonable, with more uniform internal forces and better mechanical performance.

6.2. Parametric analysis of critical buckling load

Typical variations of the critical out-plane buckling load Q_{cr}/N_y with slenderness ratio S/r_{xm} in obtained from Equation (51) are plotted in Figure 11a for shallow variable cross-sectional arches (Included angle 2Θ= 40o) and in Figure 11b for deep variable cross-sectional arches (Included angle 2Θ= 120o), where the localized parameter c/Θ=0.5, and the non-dimensional flexibility of the flexibility coefficient of elastic rotation constraint ζ =0.1.

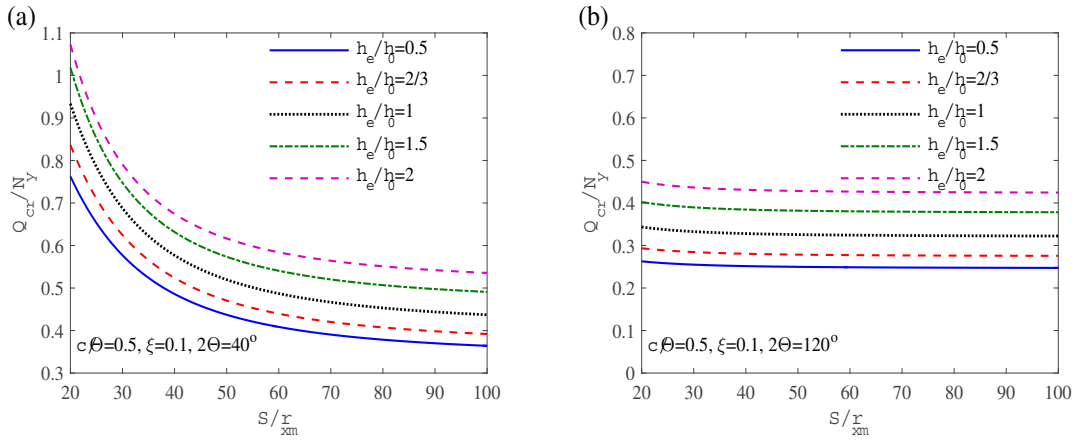

Figure 11. Influence of slenderness ratio S/r_{xm} on critical out-plane buckling load: （a）2Θ= 40º;（b）2Θ=120º.

It can be observed from Figure 11a that for shallow variable cross-sectional arches, the critical out-plane buckling load Q_{cr}/N_y decreases as the slenderness ratio S/r_{xm} increases. On the other hand, Figure 11b shows that for deep variable cross-sectional arches, the non-dimensional out-plane buckling load Q_{cr}/N_y is nearly unaffected by the slenderness ratio S/r_{xm}. Additionally, a larger cross-sectional height ratio he/h0 leads to a higher out-plane buckling load, indicating a greater structural stability.

Preprints (www.preprints.org) | NOT PEER-REVIEWED | Posted: 13 October 2023 doi:10.20944/preprints202310.0874.v1

The Figure 12 offers insight into the effects of the flexibility coefficient of elastic rotation constraint ζ on critical out-plane buckling load Q_{cr}/N_y, where the localized parameter c/Θ=0.5, and slenderness ratio S/r_{xm}=50. Figure 12a reveals that the non-dimensional out-plane buckling load of a shallow variable cross-sectional arch(Included angle 2Θ= 40o) is affected by the flexibility coefficient of elastic rotation constraint ζ, and it can be concluded from the Figure that the critical out-plane buckling load Q_{cr}/N_y decreases with the increase of the flexibility coefficient of elastic rotation constraint ζ, which is fast in the beginning and slow in the later period. However, the critical out-plane buckling load Q_{cr}/N_y of a deep variable cross-sectional arch (Included angle 2Θ= 120º) has little effect on the variation of the flexibility coefficient of elastic rotation constraint ζ as shown in Figure 12b. In addition, consistent with Figure 11, a larger cross-sectional height ratio h_e/h_0 can result in a greater critical out-plane buckling load Q_{cr}/N_y.

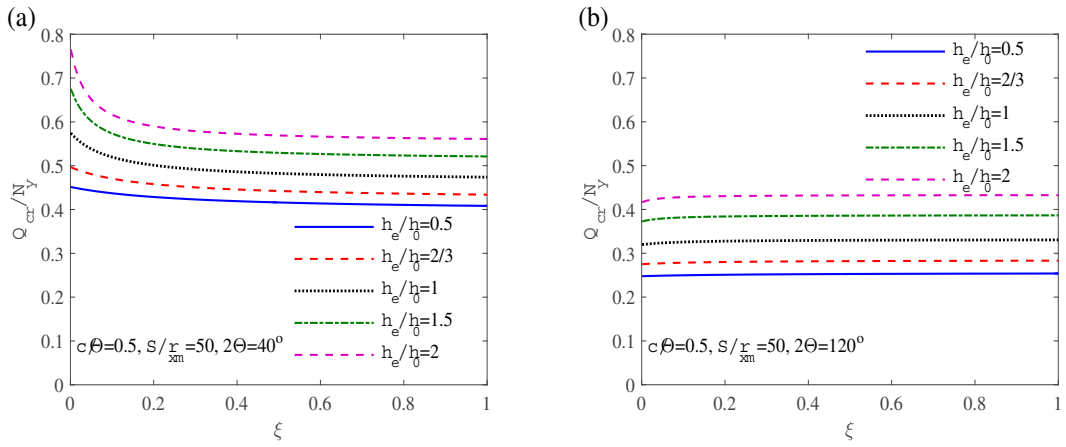

Figure 12. Influence of the flexibility coefficient of elastic rotation constraint ζ on critical out-plane buckling load：(a)2Θ= 40º; (b)2Θ=120º.

7. Conclusions

This paper presented analytical investigations on the elastic out-plane buckling of circular variable cross-sectional arches. By considering the variable cross-sectional form using the natural constant *e*, analytical solutions for the pre-buckling stresses, internal forces, and critical out-plane buckling load of the arches were obtained. The analytical solutions for pre-buckling internal forces and critical out-plane buckling load were compared with the ANSYS results, and a high level of agreement was observed between them. This demonstrates that the analytical solutions presented in this paper were capable of accurately predicting the elastic out-plane buckling behavior. In addition, by conducting parameter analysis of pre-buckling stresses, internal forces, and critical out-plane buckling load, it was found that

(1) As the cross-sectional height ratio of the variable cross-sectional arch increases, the segments of the arch axis experiencing compressive stress increase, while the segments experiencing tensile stress gradually decrease. These result in a more uniform distribution of stress in the arch.

(2) Through the analysis of the effects of the in-plane slenderness ratio S/r_{xm}, the localized parameter c/Θ, the flexibility coefficient of the flexibility coefficient of elastic rotation constraint ζ, and the variation of internal forces along the arch axis, it can be observed that compared to arches with a uniform cross-sectional height ratio h_e/h_0=1, variable cross-sectional arches with h_e/h_0 greater than 1 exhibit larger axial compression N_c/Q and smaller bending moment $4M_c/(QL)$. However, for variable cross-sectional arches with he/h0 less than 1, the axial compression N_c/Q is smaller, and the bending moment $4M_c/(QL)$ is larger. Therefore, properly designed variable cross-sectional arches exhibit more uniform internal force distribution and better pre-buckling performance.

(3) Through the parametric analysis of the critical out-plane buckling load, it has been found that compared to arches with a uniform cross-section height ratio of h_e/h_0=1, variable cross-section arches with a cross-section height ratio h_e/h_0 greater than 1 can achieve a larger critical out-plane buckling

Preprints (www.preprints.org) | NOT PEER-REVIEWED | Posted: 13 October 2023 doi:10.20944/preprints202310.0874.v1

load, indicating a higher level of stability. These findings provide valuable insights for structural design.

Author Contributions: Conceptualization, Jiang, A.F., Deng, D.Y., Dai, W., You, X.W., and Lu, H.W.; methodology, Jiang, A.F., Deng, D.Y., Dai, W., You, X.W., and Lu, H.W.; software, Jiang, A.F., Deng, D.Y., Dai, W., You, X.W., and Lu, H.W.; formal analysis, Jiang, A.F., and Lu, H.W.; investigation, Deng, D.Y., Dai, W., and Lu, H.W.; resources, Deng, D.Y., Dai, W. and Lu, H.W.; data curation, Jiang, A.F., and Lu, H.W.; writing—original draft preparation, Jiang, A.F., Deng, D.Y., Dai, W.; writing—review and editing, Jiang, A.F and Lu, H.W.; visualization, Lu, H.W.; supervision, Lu, H.W.; project administration, Lu, H.W ; funding acquisition, Lu, H.W.. All authors have read and agreed to the published version of the manuscript.

Funding: The research reported was financially supported by the National Natural Science Foundation of China (No.51908146), and the project features innovation of Guangdong Province(No.2019KTSCX190).

Data Availability Statement: The data presented in this study are available on request from the corresponding author.

Acknowledgments: The authors would like to thank all partners of School of Transportation and Civil Engineering & Architecture, Foshan University for their contribution to this research, with specific thanks to all partners in China Construction Steel Structure Guangdongcorp. ltd. Additionally , the authors thank all partners at School of Civil Engineering, Southeast University, Nanjing who have been extremely cooperative in their involvement in this research.

Conflicts of Interest: The authors declare no conflict of interest.

Appendix A- Coefficients A_{11}, A_{12}, A_{13}, A_{21}, A_{22} and A_{23}

Coefficients A_{11}, A_{12}, A_{13}, A_{21}, A_{22} and A_{23} are given by

$$A_{11}=\frac{\left[6\zeta\Theta A_0 r_{x0}^2 a+I_m\left(1-\mathrm{e}^{-3a\Theta}\right)\right]R}{3aI_m r_{x0}^2 EA_0} \tag{a1}$$

$$A_{12}=\frac{\left[(3a\cos\Theta-\sin\Theta)\mathrm{e}^{-3a\Theta}-3a\right]R^2}{EAr_{x0}^2\left(9a^2+1\right)}+\frac{2\zeta\Theta R^2(1-\cos\Theta)}{EI_m}+\frac{\left(1-\mathrm{e}^{-3a\Theta}\right)R^2}{3aEA_0 r_{x0}^2} \tag{a2}$$

$$A_{13}=qR^3\left\{\frac{\left[I_m\left(9a^2\cos c-9a^2-1\right)-6\Theta\zeta r_{x0}^2 a\left(3a^2+1\right)A\sin\Theta\sin c\right]\mathrm{e}^{3ca}+I_m}{3a\mathrm{e}^{3ca}EAr_{x0}^2\left(9a^2+1\right)I_m}\right\}+\frac{qR^3\sin c\left(3a\sin\Theta+\cos\Theta\right)}{EA\mathrm{e}^{3a\Theta}r_{x0}^2\left(9a^2+1\right)} \tag{a3}$$

$$A_{21}=\frac{\left[I_m(3a\cos\Theta-\sin\Theta)\mathrm{e}^{-3a\Theta}-A\Theta\left(18a^2+2\right)\zeta r_{x0}^2\cos\Theta-3aI_m\right]R^2}{EI_m\left(9a^2+1\right)Ar_{x0}^2} \tag{a4}$$

$$A_{22}=\frac{\left[a\mathrm{e}^{-a\Theta}(1-\beta)\left(a\sin^2\Theta+\sin(2\Theta)\right)+\left(a^2+2\beta+2\right)\left(1-\mathrm{e}^{-a\Theta}\right)\right]R}{EAa\left(a^2+4\right)}+\frac{R^3}{E}\left[\frac{2\Theta\zeta\cos\Theta}{I_m}(\cos\Theta-1)-\frac{9a^2\cos^2\Theta+2-3a\sin(2\Theta)}{3\mathrm{e}^{3a\Theta}r_{x0}^2 aA\left(9a^2+4\right)}\right]+\frac{R^3}{EAr_{x0}^2}\left[\frac{(3a\cos\Theta-\sin\Theta)\mathrm{e}^{-3a\Theta}-3a}{9a^2+1}+\frac{9a^2+2}{3\left(9a^2+4\right)a}\right] \tag{a5}$$

and

$$A_{23}=\frac{qR^2\sin c}{EA}\left\{\frac{(1-\beta)\left[\sin(2\Theta)a+2\cos(2\Theta)\right]}{2e^{a\Theta}\left(a^2+4\right)}-\frac{R^2\left[3\sin(2\Theta)a+2\cos(2\Theta)\right]}{2e^{3a\Theta}\left(9a^2+4\right)r_{x0}^2}\right\}$$
$$+\frac{qR^2}{EA}\left\{\frac{\left[(2\beta-1)a^2+2\beta+2\right]\cos c+a\left(a^2\beta+\beta+3\right)\sin c}{\mathrm{e}^{ca}a\left(a^4+5a^2+4\right)}-\frac{R^2\left[\cos c\left(9a^2-2\right)-9a\sin c\right]}{3a\left(81a^4+45a^2+4\right)r_{x0}^2\mathrm{e}^{3ca}}\right\} \quad \text{(a6)}$$
$$+\frac{qR^2}{E}\left\{\frac{R^2\Theta\zeta\sin c\sin(2\Theta)}{I_m}+\frac{\cos c}{Aa}\left[\frac{R^2\left(9a^2+2\right)}{3r_{x0}^2\left(9a^2+4\right)}-\frac{a^2+2\beta+2}{a^2+4}\right]+\frac{a}{A}\left[\frac{3R^2r_{x0}^{-2}}{9a^2+1}+\frac{1}{a^2+1}\right]\right\}$$

References

1. Trahair, N S.; *Flexural-torsional buckling of structures*, 1rd ed.; Publisher: CRC press, **1993**.
2. Liu, A.; Lu, H.; Fu, J.; et al. Analytical and experimental studies on out-of-plane dynamic instability of shallow circular arch based on parametric resonance. *Nonlinear dynamics*, **2017**, 87(1), 677-694.
3. Yuan, C.; Hu, Q.; Wang, Y.; et al. Out-of-plane stability of fixed concrete-filled steel tubular arches under uniformly distributed loads. *Magazine of Concrete Research*, **2021**, 73(18), 945-957.
4. Pi, Y L.; Bradford, M A.; Tong, G S. Elastic lateral–torsional buckling of circular arches subjected to a central concentrated load. *International Journal of Mechanical Sciences*, **2010**, 52(6), 847-862.
5. Liu, A.; Lu, H.; Fu, J.; et al. Lateral-torsional buckling of circular steel arches under arbitrary radial concentrated load. *Journal of Structural Engineering*, **2017**, 143(9), 04017129.
6. Lu, H.; Liu, A.; Bradford, M A.; et al. Experimental investigation of out-of-plane buckling of circular arches under a central radial point load. *Thin-Walled Structures*, **2020**, 148, 106198.
7. Lu, H.; Liu, A.; Pi, Y L.; et al. Flexural-torsional buckling of steel arches under a localized uniform radial-load incorporating shear deformations. *Journal of Structural Engineering*, **2019**, 145(10), 04019117.
8. Pi, Y L.; Bradford, M A. Out-plane strength design of fixed steel I-section arches. *Journal of structural engineering*, **2005**, 131(4), 560-568.
9. Guo, Y L.; Zhao, S Y.; Dou, C.; et al. Out-plane elastic buckling of circular arches with elastic end restraints. *Journal of Structural Engineering*, **2014**, 140(10), 1-9.
10. Xi, K T.; Li, J.; Zhou, T G.; et al. Out-plane Stability Analysis of U-Section Pin-End Steel Arch. *Applied Mechanics and Materials*, **2013**, 351, 169-173.
11. Pi, Y L.; Trahair, N S. Out-of-plane inelastic buckling and strength of steel arches. *Journal of Structural Engineering*, **1998**, 124(2), 174-183.
12. Bouras, Y.; Vrcelj, Z. Out-of-plane stability of concrete-filled steel tubular arches at elevated temperatures. International *Journal of Mechanical Sciences*, **2020**, 187, 105916.
13. Liu, L.; Zhang, Z.; Liu, A.; et al. Out-of-plane buckling of functionally graded porous arches reinforced by graphene platelets in a thermal environment. *Mechanics of Advanced Materials and Structures*, **2023**, 1-15.
14. Malekzadeh, P.; Karami, G. Out-of-plane static analysis of circular arches by DQM. *International journal of solids and structures*, **2003**, 40(23), 6527-6545.
15. Lim, N H.; Kang, Y J. Out of plane stability of circular arches. *International Journal of Mechanical Sciences*, **2004**, 46(8), 1115-1137.
16. Xi, K T.; Li, J.; Zhou, T G.; et al. Out-of-Plane Stability Analysis of I-Section Steel Arch. *Applied Mechanics and Materials*, **2013**, 405, 781-785.
17. Wang, X R.; Jin, J K.; Yang, G. Analysis on In-Plane and Out-Plane Instability Coupling of Steel Bowstring Arch Bridge with Box Section Single Rib. *Advanced Materials Research*, **2013**, 790, 337-340.
18. Guo, Y L.; Zhao, S Y.; Dou, C.; et al. Out-of-plane strength design of spatially trussed arches with a rectangular lattice section. *Journal of Constructional Steel Research*, **2013**, 88, 321-329.
19. Zhong, Z.; Liu, A.; Fu, J.; et al. Analytical and experimental studies on out-of-plane dynamic parametric instability of a circular arch under a vertical harmonic base excitation. *Journal of Sound and Vibration*, **2021**, 500, 116011.
20. Dou, C.; Guo, Y L.; Zhao, S Y.; et al. Elastic out-plane buckling load of circular steel tubular truss arches incorporating shearing effects. *Engineering structures*, **2013**, 52, 697-706.
21. Bouras, Y.; Vrcelj, Z. out-plane stability of concrete-filled steel tubular arches at elevated temperatures. *International Journal of Mechanical Sciences*, **2020**, 187, 105916.

22. Hayman, B.; Creep buckling—a general view of the phenomena. Creep in Structures: 3rd Symposium, Leicester, UK, September 8–12, 1980. Berlin, Heidelberg, Springer Berlin Heidelberg, **1981**, 289-307.
23. Geng, Y.; Ranzi, G.; Wang, Y T.; et al. out-plane creep buckling analysis on slender concrete-filled steel tubular arches. *Journal of Constructional Steel Research*, **2018**, 140: 174-190.
24. Shafiee, H.; Naei, M H.; Eslami, M R. In-plane and out-plane buckling of arches made of FGM. *International Journal of Mechanical Sciences*, **2006**, 48(8), 907-915.
25. Piovan, M T.; Domini, S.; Ramirez, J M. In-plane and out-plane dynamics and buckling of functionally graded circular curved beams. *Composite Structures*, **2012**, 94(11), 3194-3206.
26. Huang, C S.; Tseng, Y P.; Leissa, A W.; et al. An exact solution for in-plane vibrations of an arch having variable curvature and cross-section. *International Journal of Mechanical Sciences*, **1998**, 40(11), 1159-1173.
27. Shin, Y J.; Kwon, K M.; Yun, J H. Vibration analysis of a circular arch with variable cross-sectional using differential transformation and generalized differential quadrature. *Journal of sound and vibration*, **2008**, 309(1-2), 9-19.
28. Tsiatas, G C.; Babouskos, N G. Linear and geometrically nonlinear analysis of non-uniform shallow arches under a central concentrated force. *International Journal of Non-Linear Mechanics*, **2017**, 92, 92-101.
29. Yan, S.; Shen, X.; Chen, Z.; et al. On buckling of non-uniform shallow arch under a central concentrated load. *International Journal of Mechanical Sciences*, **2017**, 133, 330-343.
30. Yan, S.; Shen, X.; Chen, Z.; et al. On collapse of non-uniform shallow arch under uniform radial pressure. *Engineering Structures*, **2018**, 160, 419-438.
31. Liu, A.; Lu, H.; Pi, Y L.; et al. out-plane Parametric Resonance of Arches Under an In-Plane Central Harmonic Load. International Symposium on Environmental Vibration and Transportation Geodynamics. Springer, Singapore, **2016**, 45-51.
32. Bradford, M A.; Pi, Y L.; Liu, A. Out-plane elastic-plastic buckling strength of high-strength steel arches. *Journal of Structural Engineering*, **2018**, 144(6), 04018053.
33. Pi, Y L.; Trahair, N S. out-plane inelastic buckling and strength of steel arches. *Journal of Structural Engineering*, **1998**, 124(2), 174-183.